Biointerface Research in Applied Chemistry
Platinum Open Access Journal (ISSN: 2069-5837)

Article
Volume 12, Issue 6, 2022, 7804 - 7816
https://doi.org/10.33263/BRIAC126.78047816

Experimental and Quantum Mechanical Investigation of N-heterocyclic Carbene Palladium Complex: Synthesis and Antibacterial Activity

Ichraf Slimani [1], Mohamed Oussama Zouaghi [2], Nejib Jebli [3], Arfaoui Youssef [2], Namık Özdemir [4], Ismail Özdemir [5,6], Nevin Gürbüz [5,6], Lamjed Mansour [7], Khaireddine Dridi [8], Hamdi Naceur [1,*]

[1] Research Laboratory of Environmental Sciences and Technologies (LR16ES09), Higher Institute of Environmental Sciences and Technology, University of Carthage, Hammam-Lif, Tunisia, PB 77 - P.O. Box 77,1054 Amilcar
[2] Laboratory of Characterizations, Applications & Modeling of Materials (LR18ES08), Department of Chemistry, Faculty of Sciences, University of Tunis El Manar, 2092, Tunis, Tunisia
[3] Laboratory of Hetero-Organic Compounds and Nanostructured Materials (LR18ES11), University of Carthage, Faculty of Sciences of Bizerte, 7021 Jarzouna, Tunisia
[4] Department of Mathematics and Science Education, Faculty of Education, Ondokuz Mayıs University, 55139 Samsun, Turkey
[5] İnönü University, Catalysis Research, and Application Center, 44280-Malatya, Turkey
[6] İnönü University, Faculty of Science and Art, Department of Chemistry, 44280 Malatya, Turkey
[7] Zoology Department, College of Science, King Saud University, Saudi Arabia, P.O. Box 2455, Riyadh 11451, Saudi Arabia
[8] Department of Chemistry, College of Science and Arts, Qassim University, Ar Rass, 51921 Saudi Arabia
* Correspondence: naceur.hamdi@isste.rnu.tn (N.H.);

Scopus Author ID 55508562900
Received: 4.10.2021; Revised: 10.11.2021; Accepted: 14.11.2021; Published: 2.12.2021

Abstract: In this study, we report the synthesis, characterization, and biological activity of Pd-NHC-PEPPSI complex **2a**. Further confirmations of structural details were provided by a single-crystal X-ray. A single crystal of **2a** shows that the coordination geometry around Pd slightly distorted square-planar geometry. Intermolecular interactions have been studied through the NBO analyses. Structural parameters and spectroscopic properties of the complexes are well interpreted by DFT and TD-DFT calculations. Moreover, the complex **2a** showed a remarkable antimicrobial effect against *Micrococcus luteus* LB 14110mm, *Listeria monocytogenes* ATCC 19117, *Salmonella typhimurium* ATCC 14028, *Staphylococcus aureus* ATCC 6538, *Pseudomonas aeruginosa*, and *Candida albicans*.

Keywords: DFT; N-heterocyclic carbene; palladium; PEPPSI complex; X-ray crystallography.

1. Introduction

The first successful isolation and characterization of an N-heterocyclic carbene in 1991 introduced a novel category of organic compounds to the world of research [1]. From their beginnings as academic oddities, N-heterocyclic carbenes are now some of organic chemistry's most important tools, with many applications in commercially important processes. Over the last two decades, stable NHCs have been used for designing a range of catalysts employing Pd(II), Cu(I), Ni(II), Fe(0), Zn(II), Ag(I), Au(I/III), Ru(II), and Rh (I) metal-based precursors. These catalysts were utilized for different organic transformations, such as the Suzuki–Miyaura cross-coupling reaction and C–H bond activation [2–8]. Organ and co-workers reported in 2006 a new class of Pd(II) precatalysts, called Pd-PEPPSI (PEPPSI = Pyridine Enhanced Precatalyst Preparation, Stabilization, and Initiation) [9]. Pd-PEPPSI precatalysts have been shown to be

highly stable in the air allowing for easy storage and handling [10–13]. Moreover, these precatalysts have been reported as very efficient in several C-C bond-forming cross-coupling reactions [14-17].

In this paper, the results of crystal structure determination, spectroscopy, and theoretical modeling of NHC-palladium(II) complex 2a are presented and discussed. Furthermore, this complex showed a remarkable antimicrobial effect against *Micrococcus luteus* LB 14110, *Listeria monocytogenes* ATCC 19117, *Salmonella typhimurium* ATCC 14028, *Staphylococcus aureus* ATCC 6538, *Pseudomonas aeruginosa*, and *Candida albicans*.

2. Materials and Methods

2.1. General remarks.

The Pd-PEPPSI complex (**2a**) was synthesized (Scheme 1) according to the published procedure [18]. IR spectra were recorded on ATR unit in the range of 400-4000 cm^{-1} with Perkin Elmer Spectrum 100 Spectrophotometer (The samples were analyzed by transmittance with KBr because KBr has a transmittance of 100% in the range of wavenumber (4000-400). Therefore, It doesn't show or exhibit absorption in this range.). The electronic absorption spectra were recorded on a Cary-400 UV-visible spectrophotometer connected to a Cary data acquisition system using 1-cm matched silica cells.

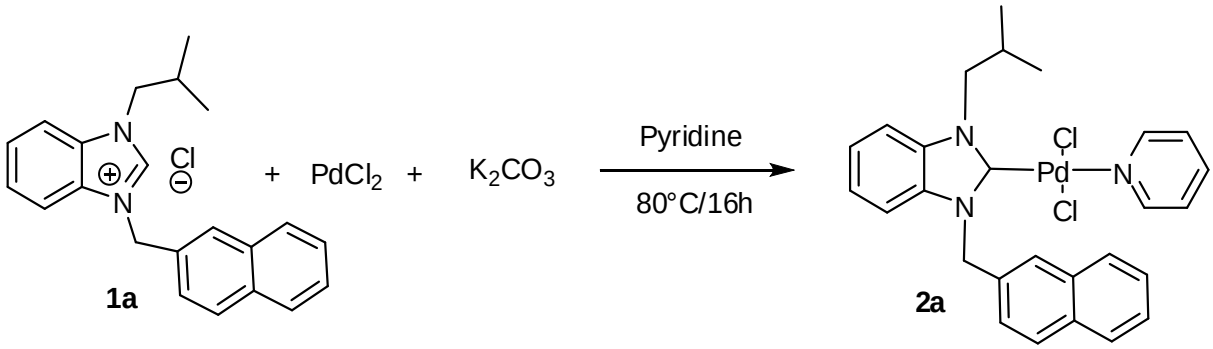

Scheme 1. Synthesis of Pd-PEPPSI complex **2a.**

2.2. X-ray crystallography.

X-ray diffraction data were collected on an STOE IPDS II diffractometer at room temperature using graphite-monochromated MoKα radiation by applying the ω-scan method. Data collection and cell refinement were carried out using X-AREA [19], while data reduction was applied using X-RED32 [19]. The structure was solved by direct methods with SIR2019 [20] and refined by means of the full-matrix least-squares calculations on F^2 using SHELXL-2018 [21]. All H atoms were located in difference maps and then treated as riding atoms, fixing the bond lengths at 0.98, 0.93, 0.97, and 0.96 Å for methine CH, aromatic CH, CH_2, and CH_3 atoms, respectively. The isopropyl methyl atom C10 was disordered over two sites, and the refined site-occupancy factors are 0.537(7)/0.463(7)%. The displacement parameters of the H atoms were fixed at U_{iso}(H) = 1.2U_{eq} (1.5U_{eq} for CH_3). Crystal data, data collection, and structure refinement details are given in Table 1. A molecular graphic was generated by using OLEX2 [22]. CCDC 2084749 contains the supplementary crystallographic data for the compound reported in this article. These data can be obtained free of charge on application to CCDC, 12 Union Road, Cambridge CB2 1EZ, UK [Fax: +44 1223 336 033, e-mail: deposit@ccdc.cam.ac.uk, https://www.ccdc.cam.ac.uk/structures/].

Table 1. Crystal data and structure refinement parameters for Pd-PEPPSI complex **2a**.

CCDC depository	2084749
Color/shape	Yellow/prism
Chemical formula	$[PdCl_2(C_{22}H_{22}N_2)(C_5H_5N)]$
Formula weight	570.81
Temperature (K)	296(2)
Wavelength (Å)	0.71073 MoKα
Crystal system	Monoclinic
Space group	$P2_1/n$ (No. 14)
Unit cell parameters	
a, b, c (Å)	9.2530(4), 12.4840(6), 21.9892(9)
α, β, γ (°)	90, 93.781(3), 90
Volume (Å^3)	2534.54(19)
Z	4
$D_{calc.}$ (g/cm^3)	1.496
μ (mm^{-1})	0.963
Absorption correction	Integration
$T_{min.}$, $T_{max.}$	0.6503, 0.8883
F_{000}	1160
Crystal size (mm^3)	0.76 × 0.19 × 0.15
Diffractometer	STOE IPDS II
Measurement method	ω scan
Index ranges	$-12 \le h \le 12, -16 \le k \le 15, -26 \le l \le 28$
θ range for data collection (°)	$1.877 \le \theta \le 27.661$
Reflections collected	14031
Independent/observed reflections	5878/3772
$R_{int.}$	0.0416
Refinement method	Full-matrix least-squares on F^2
Data/restraints/parameters	5878/44/311
Goodness-of-fit on F^2	0.882
Final R indices [$I > 2\sigma(I)$]	$R_1 = 0.0367$, $wR_2 = 0.0748$
R indices (all data)	$R_1 = 0.0721$, $wR_2 = 0.0826$
$\Delta\rho_{max.}$, $\Delta\rho_{min.}$ (e/Å^3)	0.47, −0.38

2.3. Computational studies.

All molecular calculations of optimized structures were fully optimized in the gas phase at the DFT level of theory [23-25] using a mixed basis set: 6-311G++(2d, 2p) for the H, C, N, and Cl atoms; LANL2TZ for the palladium in combination with a collection of exchange-correlation (xc) functionals: B3LYP [26-28], M06-2X [29], and ωB97X-D [30]. Also, correction for basis set superposition error (BSSE) [31] is often applied to calculating the complexation energies. With the fully optimized geometry structure, we have obtained on the succeeding the corresponding electronic structure HOMO (highest occupied molecular orbital), LUMO (lowest unoccupied molecular orbital), and the Molecular Electrostatic Potential surface [32].

In order to obtain UV absorption spectra, 30 lowest electronic excitation energies (ΔE_{0n}) and oscillator strengths (f_{0n}) were computed using the TDDFT method [33-35], again with a selection of xc functionals including global hybrids (B3LYP, M06-2X) and range-separated hybrid (ωB97X-D) and the 6-311G++(2d, 2p)/LANL2TZ mixed basis set. The optical UV absorption spectra were simulated by associating each transition with a Gaussian function having a full width at half maximum (FWHM) of 0.1 eV. The NBO analyses [36, 37] were also calculated to investigate the charge transfer between the different fragments of the Pd(II) complex. CT excitations dominated the UV absorption spectra for push-pull systems like metal complexes and were subjected to a detailed analysis [38]. Each transition is characterized by excitation energy between the ground (0) and nth excited states ($\Delta E_{opt} = \Delta E_{0n} = E_n - E_0$), and its associated transition dipole moment:

$$\mu_{0n} = \langle 0|\hat{\mu}|n\rangle \quad (1)$$

Radiative processes are governed by the oscillator strength of the transition, which is related to the transition dipole moment:

$$f_{0n} = \frac{2}{3}\Delta E_{0n}|\mu_{0n}|^2 \quad (2)$$

The CT character of the excitations can be determined from the difference of electronic density between the ground and excited states, $\Delta\rho(\vec{r})$, following the procedure described by Le Bahers *et al.* [38]. Using this method, the distance between the barycenters of the negative and positive $\Delta\rho(\vec{r})$ defines the charge-transfer distance (d_{CT}), their integration over the whole space gives the amount of charge transferred (q_{CT}), while their product gives the CT dipole moment, $\Delta\mu_{CT} = q_{CT} \times d_{CT}$.

All calculations in this work were carried out using the Gaussian 09 software package [39].

2.4. Antimicrobial activity.

2.4.1. Microorganisms, media, and growth conditions.

For the antimicrobial determination, microorganisms used as indicators were the two Gram-positive bacteria *Staphylococcus aureus* (S. aureus) ATCC6538 and *Listeria monocytogenes* (*L. monocytogenes*) ATCC 19117, the three Gram-negative bacteria *Escherichia coli* (E. coli) ATCC 8739, *Pseudomonas aeruginosa* (*P. aeruginosa*) ATCC 49189 and *Salmonella typhimurium* (*S. typhimurium*) ATCC 14028, and the fungus *Candida albicans* (*C. albicans*) ATCC 10231. All these indicator microorganisms were obtained from International Culture Collections (ATCC). The indicator microorganisms were grown overnight in Luria Bertani (LB) medium (g L^{-1}: peptone 10; yeast extract 5 and NaCl 5, pH 7.2) under aerobic condition and constant agitation (200 rpm) at 30° C for L. *monocytogenes* ATCC 19117 and *S. typhimurium* ATCC 14028 and at 37° C for *E. coli* ATCC 8739, *S. aureus* ATCC6538 and *P. aeruginosa* ATCC 49189 and then diluted 1:100 in LB media and incubated for 5 h under constant agitation (200 rpm) at the appropriate temperature. *C. albicans* ATCC 10231 was cultured at 30 °C on Sabouraud medium (g L-1: dextrose 40, peptone 10, pH 5.6) under aerobic condition and constant agitation (200 rpm) and then diluted 1:50 in Sabouraud medium and incubated for 5 h under constant agitation (200 rpm) at 30 °C.

2.4.2. Agar well diffusion method.

Agar well diffusion method was employed for the determination of the antimicrobial activity of the synthesized compounds according to Guven *et al.* (2006) [40]: Briefly, fifteen milliliters of molten agar (45 °C) were poured into sterile Petri dishes (Ø 90 mm). 50 µL of 5 h old culture of the five tested bacteria and 100 µL of 5 h old culture of the fungus *C. albicans* were evenly spread onto the surface of the agar plates of LB agar medium for bacteria and Sabouraud agar medium for *C. albicans*. Once the plates had been aseptically dried, 5 mm wells were punched into the agar with a sterile cork borer. 100 µL of a solution at 500 µg mL^{-1} of each synthesized compound were dispensed into the wells. After staying at 4 °C for 2 h, the plates were incubated at the appropriate temperature for 24 h for bacterial strains and 48 h for *C. albicans*. The antimicrobial activity was assayed by measuring the inhibition zone diameter formed around each well in millimeters.

2.4.3. Minimum inhibitory concentration (MIC).

(MIC) of the synthesized compounds and the standards ampicillin, kanamycin, and fluconazole (stock solutions at 20 mg/mL^{-1}) against the five tested bacteria and *C. albicans* fungus were determined according to Sellem *et al*. (2016) [41]. The test was performed in sterile 96-well microplates with a final volume in each microplate well of 100 µL. Stock solutions of synthesized compounds and standards were serially diluted with dimethyl sulfoxide (DMSO). To each test well, the cell suspension was added to the final inoculum concentration of 106 CFU mL^{-1} of indicator microorganism. The plates were then incubated at appropriate growth conditions of the corresponding indicator microorganism. The (MIC) was defined as the lowest concentration of the synthesized compounds and standards at which the microorganism does not demonstrate visible growth after incubation. Twenty-five µl of Thiazolyl Blue Tetrazolium Bromide (MTT) at 0.5 mg mL^{-1} were added to the wells and incubated at room temperature for 30 min. The colorless tetrazolium salt acted as an electron acceptor and was reduced to a red-colored formazan product by the indicator microorganisms. When microbial growth was inhibited, the solution in the well remained clear after incubation with MTT.

For the antimicrobial activity determination (inhibition zones and CMIs), each experiment was carried out simultaneously three times under the same conditions. The diameters of inhibition zones reported in mm and the MIC values reported in µg mL-1 were similar, and the reported results are the average of the three experiments.

3. Results and Discussion

3.1. Theoretical study.

3.1.1. Structural study.

Firstly, we have investigated the impact of the xc functionals on the geometric data of the $Pd(II)-$ PEPPSI complex sketched in Figure 1.

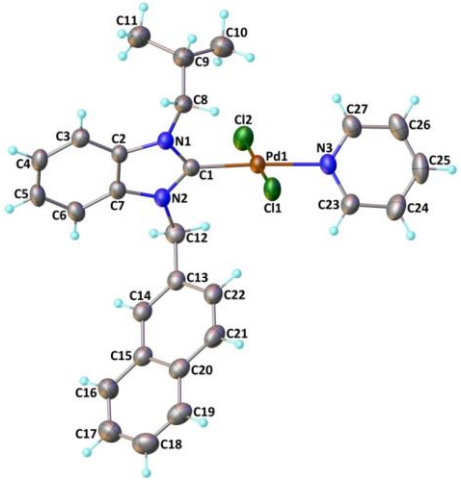

Figure 1. Molecular structure of Pd-PEPPSI complex **2a** drawn at 30% probability level.

Table 2. Geometric parameters (Bond lengths (Å) and angles (°)) determined experimentally by X-ray diffraction (XRD) and computed at several XC functionals.

Parameter	XRD	$B3LYP$	$\omega B97X-D$	$M06-2x$
Pd1-Cl2	2.299	2.427	2.403	2.433
Pd1-Cl3	2.298	2.427	2.403	2.433
Pd1-N4	2.091	2.138	2.118	2.159

Parameter	XRD	$B3LYP$	$\omega B97X-D$	$M06-2x$
Pd1-C10	1.964	1.998	1.984	1.974
Cl2-Pd1-Cl3	179.1	175.9	175.7	173.9
N4-Pd1-C10	177.0	179.4	180.0	179.8

The analysis of Table 2 shows that $\omega B97X-D$ (which comprised of 22% Hartree-Fock exchange at the short-range and 100% Hartree-Fock at the long-range) is the most suitable XC functional to optimize the Pd − PEPPSI complex. The computed geometric parameters at $\omega B97X-D$ level are close to those determined by the X-Ray diffraction method (Figure 2).

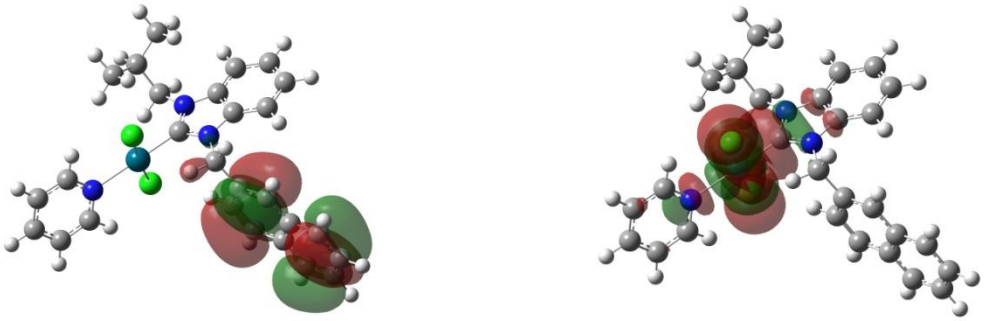

(a) (b)

Figure 2. Localization of frontier molecular orbitals of the complex **2a** : (a) HOMO (b) LUMO.

In the case of complex **2a**, the HOMO is localized on the naphthalene group, whereas the LUMO is localized on the Pd and the sites concerned with the charge transfer (Figure 3).

3.1.2. Charge-transfer character.

In order to investigate the charge transfer between the metal $(Pd(II))$ and its four ligands, we have analyzed the NBO populations before and after the complexation.

To achieve this objective, we have considered an amount of charge q_i for the three ligands of the *complex* **2a** such as explained in Figure 3.

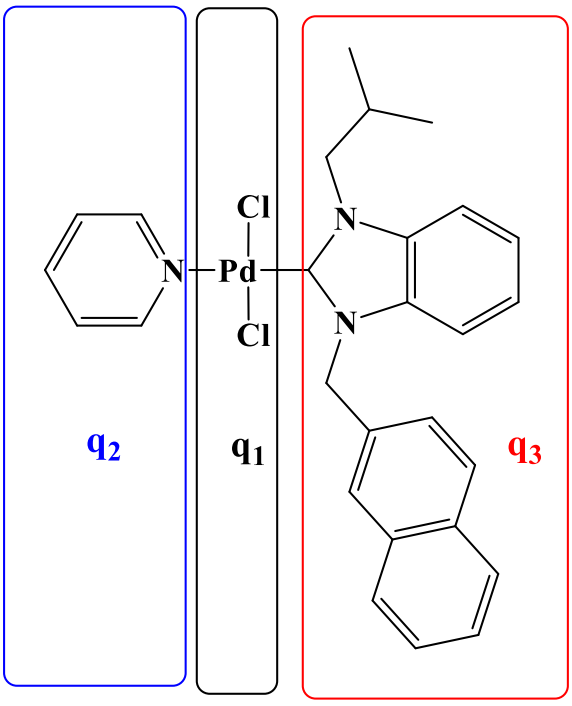

Figure 3. Repartition of the amount of charge q_i in complex **2a.**

Table 3. Computed amount charge (q_i) (e) for the three considered ligands of the complex 2a.

	Before the complexation			**After the complexation**		
Charge amount q_i	q_1	q_2	q_3	q_1	q_2	q_3
	0.000	0.000	0.000	-0.733	0.237	0.496

Table 4. Natural electron configuration of Pd(II) complex at ωB97X-d/6-311G++(2d, 2p)/LANL2TZ.

Site	**Natural Electron Configuration**
Pd1	[core]5S(0.35)4d(8.97)5p(0.38)5d(0.01)
Cl2	[core]3S(1.90)3p(5.61)
Cl3	[core]3S(1.90)3p(5.60)
N4	[core]2S(1.32)2p(4.12)3p(0.02)
C10	[core]2S(0.98)2p(2.59)3S(0.01)3p(0.03)

Table 5. Charge transfer parameters of the lowest-energy dominant excitations of selected TT derivatives [q_{CT} (e), d_{CT} (Å), $\Delta\mu_{CT} = q_{CT} \times d_{CT}$ (D)] as calculated at the TDDFT/B3LYP/6-311G++(2d,2p)/LANL2TZ level.

Compound	**Excite state number**	**q_{CT}**	**d_{CT}**	**μ_{CT}**
Complex 2a	1	0.722	0.174	0.603

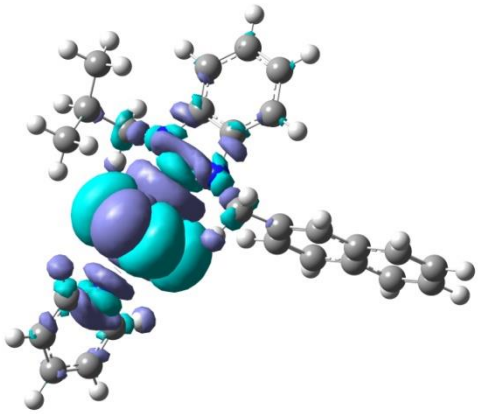

Figure 4. Excitation-induced B3LYP/6-311G++(2d, 2p)/LANL2TZ total electron density difference [$\Delta\rho(\vec{r}) = \rho_{excited}(\vec{r}) - \rho_{ground}(\vec{r})$, isocontour value 0.0004 au] for the lowest-energy excited state of Pd(II) complex. (Purple: Positive value/Light Blue: Negative value).

The analysis of Table 3 shows the charge transfer between the three fragments of the complex **2a**. We have found a main charge transfer from the imidazole derivative to the $PdCl_2$ fragment with an amount of charge (q_3 = 0.496e). Also, we have reported a second charge transfer from the pyridine ligand to $PdCl_2$ with an amount of charge (q_2 = 0.237e). Furthermore, the analysis of table 4 showed that the valence electron configurations of Pd1 and N4 confirm an important charge transfer from fragment 3 to palladium. Also, the examination of data of Table 5 showed a CT between the ground and the excited state with an amount of charge q_{CT} (0.722e).

3.1.3. Analysis of Infra-Red and Ultra-violet absorption spectra.

The experimental (in solid-state) and theoretical (in vacuum) IR spectra of the Pd(II) complex are given in Figures 5 and 6.

The bands recorded at 2975-3237 cm^{-1} are attributed to CH_2 and CH_3 stretching vibrations. In addition, the aromatic C═C stretching vibration is seen at 1639, 1650, and 1674 cm^{-1}.

UV–vis studies were employed to confirm the formation of Pd-PEPPSI complex **2a**, and the results were provided in Figure 6 and Table 6. In the case of the Carbene-Pd(II)

complex, two UV peaks are revealed [42,43], and the obtained results at the B3LYP level are in good agreement with the literature.

We have assigned the two obtained UV peaks as follows: The characteristic π -π* transition of aromatic rings moiety appeared at around λ_{max} of 273 nm [42]. On the other hand, a broad hump appeared at 314 nm due to the presence of d–d transition (metal to ligand charge transfer—MLCT) of Pd (II) [44]. The MLCT has been confirmed by the NBO analyses and the charge transfer between the ground and excited states.

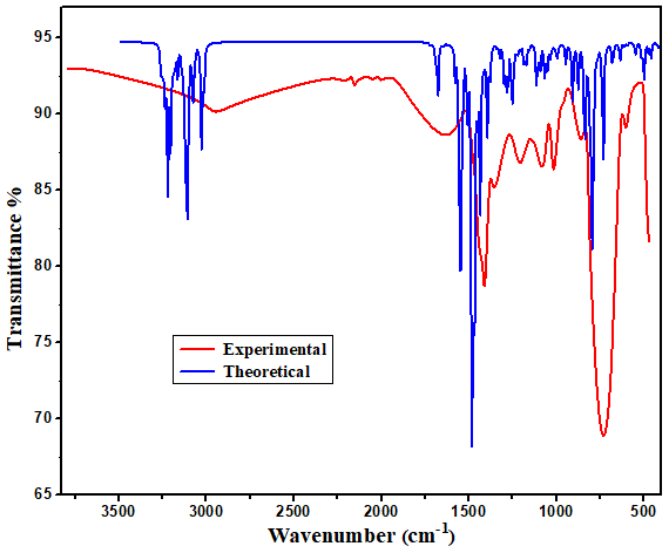

Figure 5. Experimental and computed IR spectra of complex **2a.**

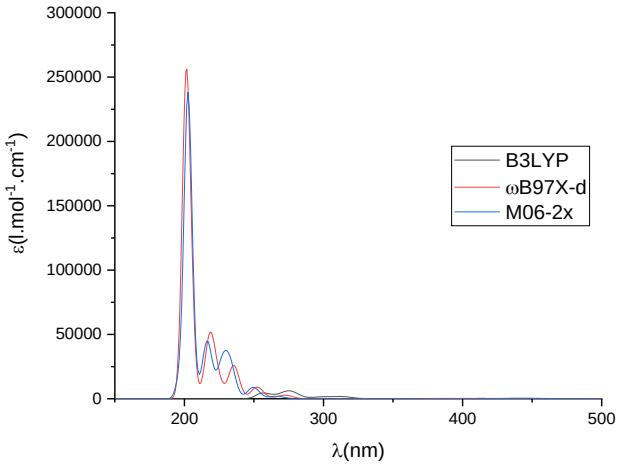

Figure 6. Computed UV absorption spectra of the complex **2a** at the level of XC functionals.

Table 6. Lowest-energy dipole-allowed excited states of complex **2a** evaluated at the level of several XC functionals [excitation energies (ΔE_{0n}, eV), the wavelength of absorption (λ_{TDDFT}, nm, as obtained from the simulated spectra), dominant MO pairs describing the excitations and oscillator strengths.

XC Functional	λ(nm)	MOs	ΔE_{0n}	f_{0n}
Experimental [41]	314			
	263			
B3LYP	314	H(-7)-L(77%)	3.94	0.01
	273	H-L(+3) (65%)	4.53	0.03
ωB97X-D	272	H(-7)-L (87%)	4.45	0.02
	252	H-L(+2) (82%)	4.91	0.07
	235	H(-4)-L(+3) (44%)	5.26	0.16
	224	H(-4)-L (12%)	5.52	0.06
		H(2-)L(+3) (14%)		

XC Functional	λ(nm)	MOs	ΔE_{0n}	f_{0n}
M06-2X	267	H(-6)-L	4.64	0.01
	249	H(-1)L(+2)	4.97	0.06
	233	H(-3)-L(+3)	5.32	0.18
	227	H(-9)-L	5.45	0.19

4. Biological activities

The Pd-NHC-PEPPSI complex **2a** was investigated for antibacterial against both grams (+)/(−) bacterias. The tests were carried out at a concentration of 0.5 mg/mL of the test sample with standard AMC. As reported earlier, DMSO did not exhibit any antimicrobial activity [45,46]. The antimicrobial activities of the Pd-NHC-PEPPSI complex **2a** are summarized in Table 7

The Pd-NHC-PEPPSI complex **2a** tested in this study for its antimicrobial activity displayed a very good performance. Compound **2a** showed good activity against all types of bacteria especially, *Micrococcus luteus* LB 14110: 24±2.17 mm (with significant difference of $P < 0.01$ in comparison to positive control), *Listeria monocytogenes* ATCC 19117: 25±2.12mm, *Salmonella typhimurium* ATCC 14028: 26±2.15 mm, *Staphylococcus aureus* ATCC 6538: 25±2.11 mm, *Pseudomonas aeruginosa*: 28±2.11 mm and *Candida albicans* 26±2.13 mm.

Table 7. Zone of bacterial inhibition measured in mm of Pd-NHC-PEPPSI **2a.**

Micro organisms **Product**	***Micrococcus luteus*** **LB 14110**	***Listeria monocytogenes*** **ATCC 19117**	***Salmonella Typhimurium*** **ATCC 14028**	***Staphylococcus aureus*** **ATCC 6538**	***Pseudomonas aeruginosa***	***Candida albicans***
2a	24±2.17*	25±2.12*	26±2.15*	25±2.11*	28±2.11*	26±2.13*
AMC	25±2.1*	24±2.2*	23±2.3*	21±2.1*	20±2.2*	20±2.*

This table indicates the antibacterial activities of the tested compound in inhibition zones by mm. The values are means ± S.D. AMC (ampicillin) was used as a positive control drug. * $P < 0.01$.

4.1. Minimum inhibitory concentration (MIC) determination.

Minimum inhibitory concentration (MIC) of the synthesized compound **2a** and the standard ampicillin were assessed using the microdilution method against three indicator microorganisms: the two Gram-positive bacteria *L. monocytogenes* and *S. aureus*, the Gram-negative bacterium *S. typhimurium* ATCC 14028.

The antibacterial activity of the Pd-NHC-PEPPSI complex **2a** is reported in the minimum inhibitory concentration (MIC) values, which are the lowest concentration of an antimicrobial compound that visibly inhibits the growth of the bacteria after overnight incubation. The antimicrobial activity of complex **2a** was evaluated against *Listeria monocytogenes* ATCC 19117, *Salmonella typhimurium* ATCC 14028, and *Micrococcus luteus* and was compared with ampicillin. All were used to treat general bacterial infections. The MIC value of the tested complex is presented in Table 8.

The MICs values range from 0.125 to 1.15 mg mL-1 against *Listeria monocytogenes* ATCC 19117, *Salmonella Typhimurium* ATCC 14028, and *Micrococcus luteus*. The lowest MIC value was obtained against *Listeria monocytogenes* ATCC 19117. The Pd-NHC-PEPPSI complex **2a** showed a weak performance compared with ampicillin.

Table 8. The minimal bacterial inhibitory concentration measured in mg/mL of Pd-PEPPSI complex **2a**.

Microorganism indicator	Compound	MIC (mg/ml)
Listeria monocytogenes ATCC 19117	**2a**	0.125±0.11
	Ampicillin	0.039±0.12
Salmonella Typhimurium ATCC 14028	**2a**	1.15±0.12
	Ampicillin	0.039±0.11
Micrococcus luteus	**2a**	0.325±0.12
	Ampicillin	0.039±0.12

This table indicates the Minimal bacterial inhibitory concentration of the tested compound **2**. The values are means ± S.D. AMC (ampicillin) was used as a control positive drug. * P < 0.01.

5. Conclusions

In conclusion, Pd-NHC-PEPPSI complex **2a** was synthesized and characterized by IR, UV, X-ray, and molecular modeling techniques. Computational studies on the structural and spectroscopic features of the complex were done at the DFT level of theory. Furthermore, The Pd-NHC-PEPPSI complexes **2a** showed better antimicrobial activity than the AMC (ampicillin).

Funding

This research received no external funding.

Acknowledgments

This work was supported by the Research Supporting Project (RSP- 2021/75), King Saud University (Riyadh, Saudi Arabia).

Conflicts of Interest

The authors declare no conflict of interest.

References

1. Arduengo III, A.J.; Harlow, R.L.; Kline, M. A. Stable crystalline carbene. *J Am Chem Soc* **1991**, *113*, 361-363, https://doi.org/10.1021/ja00001a054.
2. Lei, P.; Meng, G.; Ling, Y.; An, J.; Szostak, M. Pd-PEPPSI: Pd-NHC precatalyst for Suzuki–Miyaura cross-coupling reactions of amides. *J Org Chem* **2017**, *82*, 6638-6646, https://doi.org/10.1021/acs.joc.7b00749.
3. Li, G.; Lei, P.; Szostak, M.; Casals-Cruañas, E.; Poater, A.; Cavallo, L.; Nolan, S.P. Mechanistic Study of Suzuki–Miyaura Cross-Coupling Reactions of Amides Mediated by [Pd (NHC)(allyl) Cl] Precatalysts. *ChemCatChem* **2018**, *10*, 3096-3106, https://doi.org/10.1002/cctc.201800511.
4. Kaloğlu, N.; Özdemir, İ. PEPPSI-Pd-NHC catalyzed Suzuki-Miyaura cross-coupling reactions in aqueous media. *Tetrahedron* **2019**, *75*, 2306-2313, https://doi.org/10.1016/j.tet.2019.02.062.
5. Waseem, M., Rami, S., Wissam, I., Mohammed, F., El Ali, B. Synthesis, crystal structure, and catalytic activity of bridged-bis (N-heterocyclic carbene) palladium(II) complexes in selective Mizoroki-Heck cross-coupling reactions. *Polyhedron* **2021**, *207*, *115371*, https://doi.org/10.1016/j.poly.2021.115371.
6. Sofie, M.P.; Vanden, B.; Catherine, S.J. Cazin, Manganese-N-heterocyclic carbene (NHC) complexes – An overview. *Polyhedron* **2021**, *205*, *115371*, https://doi.org/10.1002/cctc.201800241.

7. Katagiri, T.; Amao, Y. Recent advances in light-driven C–H bond activation and building C–C bonds with CO 2 as a feedstock for carbon capture and utilization technology. *Green Chemistry* **2020**, *22*, 6682-6713, https://doi.org/10.1039/D0GC01796E.
8. Shariatipour, M.; Salamatmanesh, A.; Nejad, M.J.; Heydari, A. Imidazole-aryl coupling reaction via CH bond activation catalyzed by palladium supported on modified magnetic reduced graphene oxide in alkaline deep eutectic solvent. *Catal Commun* **2020**, 135, *105890*, https://doi.org/10.1016/j.catcom.2019.105890.
9. Can, H.; Jiahao, L.; Hai-Hua, H.; Zhuofeng, K. Recent progress in electro- and photo-catalytic CO2 reduction using N-heterocyclic carbene transition metal complexes. *Polyhedron* **2021**, 203, *115147*, https://doi.org/10.1016/j.poly.2021.115147.
10. Gokanapalli, A.; Motakatla, V.K.R.; Peddiahgari, V.G.R.. Investigation of Pd-PEPPSI catalysts and coupling partners towards direct C2-arylation/heteroarylation of benzoxazole. *Appl Organomet Chem* **2021**, e6296, https://doi.org/10.1002/aoc.6296.
11. Guillet, S.G.; Voloshkin, V.A.; Saab, M.; Beliš, M.; Van Hecke, K.; Nahra, F.; Nolan, S.P. Understanding existing and designing novel synthetic routes to Pd-PEPPSI-NHC and Pd-PEPPSI-PR 3 precatalysts. *ChemComm* **2020**, *56*, 5953-5956, https://doi.org/10.1039/D0CC02262D.
12. Aziza, M.; Abdullah, S. A.; Ismail, Ö.; Nevin, G.; Hamdi, N. A new PEPPSI type N-heterocyclic carbene palladium(II) complexes and its efficiency as a catalyst for Mizoroki-Heck cross-coupling reactions in water : Synthesis, Characterization and their antimicrobial and Cytotoxic activities. *Journal of Molecular Structure* **2021**, 234, *130204*, https://doi.org/10.1016/j.molstruc.2021.130204.
13. Miroslav, D.; Petar, P.; Nikolay, G.V. N-heterocyclic bis-carbene palladium complexes derived from functionalized naphthalimides – Synthesis, Structure elucidation and DFT study. *Journal of Molecular Structure* **2021**, 1230, 129944, https://doi.org/10.1016/j.molstruc.2021.129944.
14. Ceren, A.; Namık, O.; Mert, O. K.; Bülent, A.; Ismail, O. Synthesis, crystal structures and catalytic activities of palladium complexes with coumarin-functionalised N-heterocyclic carbene ligands, *Inorganic Chemistry Communications* **2021**, 131, *108755*, https://doi.org/10.1016/j.inoche.2021.108755.
15. Ahmadvand, Z.; Bayat, M.; Zolfigol, M.A. Toward prediction of the precatalyst activation mechanism through the cross-coupling reactions: Reduction of Pd (II) to Pd (0) in precatalyst of the type Pd-PEPPSI. *J Comput Chem* **2020**, *41*, 2296-2309, https://doi.org/10.1002/jcc.26393.
16. Borah, D.; Saha, B.; Sarma, B.; Das, P. A new PEPPSI type N-heterocyclic carbene palladium (II) complex and its efficiency as a catalyst for Mizoroki-Heck cross-coupling reactions in water. *J Chem Sci* **2020**, *132*, 1-10, https://doi.org/10.1007/s12039-020-1754-y.
17. Kumar, A.; Kumar, M.; Verma, A.K. Well-Defined Palladium N-Heterocyclic Carbene Complexes: Direct C–H Bond Arylation of Heteroarenes. *J Org Chem* **2020**, *85*, 13983-13996, https://doi.org/10.1021/acs.joc.0c02024.
18. Slimani, I.; Mansour, L.; Özdemir, I.; Gürbüz, N.; Hamdi, N. Synthesis, characterization and catalytic activity of PEPPSI-type palladium–NHC complexes. *Inorganica Chim. Acta* **2021**, *515*, 120043, https://doi.org/10.1016/j.ica.2020.120043.
19. Nagaraju, P.; Varnakumar, G.; Debasis, S. N-heterocyclic carbene bearing thermoresponsive poly(NIPAM) supported palladium (II) complex: Synthetic strategy and application. *Journal of Organometallic Chemistry* **2020**, *913*, 121196.
20. Mert, O.K. Comparison of the catalytic performances of bridged bi-metallic and nonbridged mono-metallic PEPPSI type palladium N-heterocyclic carbene complexes. *Inorganic Chemistry Communications* **2021**, 116, *107890*, https://doi.org/10.1016/j.inoche.2020.107890.
21. Thomas, S.; Enrica, B.; Isabella, C.; Flavio, R.; Nicola, D.; Fabiano, V. Synthesis and comparative study of the anticancer activity of g3 -allyl palladium(II) complexes bearing N-heterocyclic carbenes as ancillary ligands. *Polyhedron* **2020**, *186*, 114607, https://doi.org/10.1016/j.poly.2020.114607.
22. Murat, K.; Serpil, D.D.; Ismail, O. The first used butylene linked bis(N-heterocyclic carbene)-palladiumPEPPSI complexes in the direct arylation of furan and pyrrole. *Journal of Organometallic Chemistry* **2020**, *915*, 121236, https://doi.org/10.1016/j.jorganchem.2020.121236.
23. Waseem, M.; Rami, S.; Mohammed, F.; and Bassam, El Ali. Soft Heteroleptic N-Heterocyclic Carbene Palladium(II) Species for Efficient Catalytic Routes to Alkynones via Carbonylative Sonogashira Coupling *ACS Omega* **2020**, *5*, 23687−23702.
24. Koy, M., Bellotti, P., Das, M. N-Heterocyclic carbenes as tunable ligands for catalytic metal surfaces. *Nat Catal* **2021** , *4*, 352–363, https://doi.org/10.1038/s41929-021-00607-z.

25. Paulina, B.; Katarzyna, S.; Wioletta, K., Michał, M. Acenaphthene-Based N-Heterocyclic Carbene Metal Complexes: Synthesis and Application in Catalysis. *Catalysts* **2021**, *11*, 972, https://doi.org/10.3390/catal11080972.
26. Waseem M.; Rami Suleiman, Mohammed Fettouhi, and Bassam El Ali, Soft Heteroleptic N-Heterocyclic Carbene Palladium(II) Species for Efficient Catalytic Routes to Alkynones via Carbonylative Sonogashira Coupling, *ACS Omega* **2020**, 22, *5*, 23687–23702.
27. Omrani, R.; Zouaghi, M.O.; Arfaoui, Y. Mechanistic density functional theory study of the Claisen Rearrangement Diels-Alder Cycloaddition domino sequence for the synthesis of the caged garcinia xanthone. *J Mol Struct* **2020**, *1202*, 127305, https://doi.org/10.1016/j.molstruc.2019.127305.
28. Chebbi, M.; Arfaoui, Y. Reactivity of pyrazole derivatives with halomethanes: A DFT theoretical study. *J Mol Model* **2018**, *24*, 1-10, https://doi.org/10.1007/s00894-018-3718-4.
29. Nida, I.; Munazzah, Y.; Mehwish, J.; Mahvish, A.; Javed, I. Muhammad, A.I. Synthesis in combination with Biological and Computational evaluations of selenium-N-Heterocyclic Carbene compounds. *Computational and Theoretical Chemistry* 1197, **2021**, *113135*, https://doi.org/10.1016/j.comptc.2020.113135.
30. Ibrahim, A.; Nedra, T.; Waleed, K.; Tariq, K.; Ismail, Ö.; Sedat, Y.; Naceur, H. Biological Activities of NHC–Pd(II) Complexes Based on Benzimidazolylidene N-heterocyclic Carbene (NHC) Ligands Bearing Aryl Substituents. *Catalysts* **2020**, *10*, 1190, https://doi.org/10.3390/catal10101190.
31. Sylwia, O.; Thomas, S.; Steven, P.N. N-Heterocyclic carbene complexes enabling the α-arylation of carbonyl compounds. *Chem. Commun* **2021**, *57*, 4354-4375, https://doi.org/10.1039/D1CC00913C.
32. Gara, R. ; Zouaghi, M.O.; ALshandoudi, L.M.H. ; Arfaoui, Y. DFT investigation of solvent, substituent, and catalysis effects on the intramolecular Diels-Alder reaction. *J Mol Model* **2021**, *27*, 1-12, https://doi.org/10.1007/s00894-021-04729-w.
33. Casida, M.E.; Time-dependent density functional response theory for molecules. World Scientific, Singapore In Recent Advances In Density Functional Methods: (Part I) **1995**, *1*, 155-192, https://doi.org/10.1142/9789812830586_0005.
34. Bauernschmitt, R.; Ahlrichs, R.. Treatment of electronic excitations within the adiabatic approximation of time dependent density functional theory. *Chem Phys Lett* **1996**, *256*, 454-464, https://doi.org/10.1016/0009-2614(96)00440-X.
35. Tozer, D.J.; Handy, N.C. Improving virtual Kohn–Sham orbitals and eigenvalues: Application to excitation energies and static polarizabilities. *J Chem. Phys* **1998**, *109*, 10180-10189, https://doi.org/10.1063/1.477711.
36. Glendening, E.; Reed, A. E.; Carpenter, J. A.; Weinhold, F. NBO Version 3.1.
37. Zouaghi, M.O.; Doggui, M.Y.; Arfaoui, Y. Regio- and stereoselectivity of the [3+2] cycloaddition of nitrones with methyl-acetophenone: A DFT investigation. *Journal of Molecular Graphics & Modelling* **2021**, *107*, 107960, https://doi.org/10.1016/j.jmgm.2021.107960.
38. Le Bahers, T. ; Adamo, C.; Ciofini, I. A qualitative index of spatial extent in charge-transfer excitations . *J Chem Theory Comput* **2011**, *7*, 2498-2506, https://doi.org/10.1021/ct200308m.
39. Gaussian 09, Revision A. 02, Frisch, M.J.; Trucks, G.W.; Schlegel, H.B.; Scuseria, G.E.; Robb, M.A.; Cheeseman, J.R.; Scalmani, G.; Barone, V.; Petersson, G.A.; Nakatsuji, H.; Li, X.; Caricato, M.; Marenich, A.; Bloino, J.; Janesko, B. G.; Gomperts, R.; Mennucci, B.; Hratchian, H. P.; Ortiz, J. V.; Izmaylov, A. F.; Sonnenberg, J. L.; Williams-Young, D.; Ding, F.; Lipparini, F.; Egidi, F.; Goings, J.; Peng, B.; Petrone, A.; Henderson, T.; Ranasinghe, D.; Zakrzewski, V. G.; Gao, J.; Rega, N.; Zheng, G.; Liang, W.; Hada, M.; Ehara, M.; Toyota, K.; Fukuda, R.; Hasegawa, J.; Ishida, M.; Nakajima, T.; Honda, Y.; Kitao, O.; Nakai, H.; Vreven, T.; Throssell, K.; Montgomery, J. A.; Jr., Peralta, J. E.; Ogliaro, F.; Bearpark, M.; Heyd, J. J.; Brothers, E.; Kudin, K.N.; Staroverov, V.N.; Keith, T.; Kobayashi, R.; Normand, J.; Raghavachari, K.; Rendell, A.; Burant, J. C.; Iyengar, S. S.; Tomasi, J.; Cossi, M.; Millam, J. M.; Klene, M.; Adamo, C.; Cammi, R.; Ochterski J.W.; Martin, R.L.; Morokuma, K.; Farkas, O.; Foresman, J.B.; Fox, D.J. Gaussian, Inc., Wallingford CT, **2016**.
40. Guven, K., Yucel, E., and Cetintas, F., Antimicrobial activities of fruits of Crataegus and Pyrus species .Pharm. Biol. **2006**,44, 79–83, https://doi.org/10.1080/13880200600591253.Fernandes CJ, Stevens DA, Groot obbink DJ, Ackerman VP. A replicator method for the combined determination of minimum inhibitory concentration and minimum bactericidal concentration. *J Antimicrob Chemother* **1985** ,*15*, 53-60, https://doi.org/10.1093/jac/15.1.53.
41. Özdemir, N.; Touj, N.; Yaşar, S.; Hamdi, N.; Özdemir, İ. Experimental and quantum mechanical investigation on two N-heterocyclic carbene palladium complexes. *Mol Cryst Li*. Cryst **2021**, *714*, 26-36, https://doi.org/10.1080/15421406.2020.1848256.

42. Gayathri, V. ; Pentela, N. ; Samanta, D. Palladium nanoparticles capped by thermoresponsive N-heterocyclic carbene: Two different approaches for a comparative study. *Appl Organomet Chem* **2021**, *35*, e6166, https://doi.org/10.1002/aoc.6166.
43. Makharza, S.; Auisa, J.; Sharkh, S.A.; Ghabboun, J.; Faroun, M.; Dweik, H.; Sultan, W.; Sowwan, M. Structural and thermal analysis of copper-doped poly (n-isopropylacrylamide) films. *Int J Polym Anal Ch* **2010**, *15*, 254-265, https://doi.org/10.1080/10236661003747031.
44. Slimani, I.; Mansour, L.; Özdemir, I.; Gürbüz, N.; Hamdi, N. Synthesis, characterization and catalytic activity of PEPPSI-type palladium–NHC complexes. Inorganica Chim Acta **2021**, *515*, 120043, https://doi.org/10.1016/j.ica.2020.120043.
45. Shahini, C.R.; Achar, G.; Budagumpi, S.; Tacke, M.; Patil, S.A. Non–symmetrically p–nitrobenzyl–substituted N–heterocyclic carbene–silver (I) complexes as metallopharmaceutical agents. *Appl Organomet Chem* **2017**, *31*, e3819, https://doi.org/10.1002/aoc.3819.
46. Song, X.R.; Zheng, Y.; He, G.; Yang, L.; Luo, Y.F.; He, Z.Y.; Li, S.Z.; Li, J.M.; Yu, S.; Luo, X.; Hou, S.X. Development of PLGA nanoparticles simultaneously loaded with vincristine and verapamil for treatment of hepatocellular carcinoma. *J Pharm Sci* **2010**, *99*, 4874-4879, https://doi.org/10.1002/jps.22200.